Phytochemistry 69 (2008) 1989–1996

Contents lists available at ScienceDirect

Phytochemistry

journal homepage: www.elsevier.com/locate/phytochem

Pathogenesis-related proteins in somatic hybrid rice induced by bacterial blight

Chu L. Yu [a], Shun P. Yan [b], Chang C. Wang [a], Hai T. Hu [a], Wei N. Sun [b], Cheng Q. Yan [c], Jian P. Chen [c], Ling Yang [a,*]

[a] College of Chemistry and Life Sciences, Zhejiang Normal University, Jinhua, China
[b] Institute of Plant Physiology and Ecology, Shanghai Institutes for Biological Sciences, Chinese Academy of Sciences, Shanghai, China
[c] Zhejiang Academy of Agricultural Sciences, Hangzhou, China

ARTICLE INFO

Article history:
Received 2 July 2007
Received in revised form 20 October 2007
Available online 3 June 2008

Keywords:
Somatic hybrid rice
Leaf blades
Bacterial blight
Proteomics

ABSTRACT

Rice bacterial blight, caused by *Xanthomonas oryzae* pv. *Oryzae* (*Xoo*), is one of the most serious rice diseases worldwide. The bacterial blight resistance trait from *Oryza meyeriana*, a wild rice species, was introduced into an elite *japonica* rice cultivar using asymmetric somatic hybridization. This study was carried out with the intention of understanding the molecular mechanism of incompatible interaction between *Xoo* and the stable somatic hybrids by using proteomic analyses. Proteins were extracted from leaves at 24, 48, and 72 h after *Xoo* inoculation and separated by 2-DE. A total of 77 protein spots changed their intensities significantly ($p < 0.05$) by more than 1.5-fold at least at one time point. Sixty-four protein spots were successfully identified by MS analysis. Among them, 51 were known to be involved in photosynthesis. Up-regulation of Rubisco large subunit (RcbL) small fragments and down-regulation of RcbL big fragments indicated that intact RcbL and RcbL big fragments degraded following *Xoo* attack, which was further confirmed by Western blot analysis. The differential expression of proteins related to signal transduction, antioxidant defense, photosynthesis, metabolism, and protein turnover during the *Xoo* infection, suggests the existence of a complex regulatory network in the somatic hybrid rice that increases resistance toward *Xoo* infection and damage.

1. Introduction

Plants often associate with a rich diversity of microorganisms throughout the duration of their life cycle. The most obvious and well studied plant–microbe interactions are those that result in disease (Smith et al., 1999). In plants, robust defense responses to invading phytopathogens often conform to a gene-for-gene model: plant resistance will occur only when a plant possesses a dominant resistant gene (*R*) and the pathogen expresses the complementary dominant avirulence gene (*Avr*) (Hammond-Kosack and Parker, 2003). In general, rice cultivars that possess *R* gene show incompatible interaction against invading pathogen that have corresponding *Avr* gene. The incompatible interaction resulted in the hypersensitive response and the activation of rapid and effective defense responses, including the production of pathogenesis-related proteins, oxidative enzymes and phytoalexins (Hammond-Kosack and Parker, 2003; Li et al., 2006).

To gain complete understanding of molecular mechanisms underlying host–pathogen interactions, it is required to identify all signaling components from multiple biochemical pathways that are activated by the pathogen. With recent advances in technologies, there has been considerable progress in identifying global changes in gene expression during pathogen attack (Chivasa et al., 2006; Li et al., 2006). However, quantitative mRNA data do not offer insights into the quantity and quality of the final gene products, i.e. proteins, the key player in the cell. The amount of proteins is not always correlated to that of mRNA, especially for proteins of low abundance. Moreover, many proteins undergo post-translational modifications, which are extremely important for protein activities and subcellular localization (Yan et al., 2006). Therefore, it is necessary to use proteome-based expression profiling to study plant–pathogen interactions. Until now, proteomic studies associated with plant pathogenesis are focused on fungal pathogen–plant interactions (Konishi et al., 2001; Kim et al., 2004; Chivasa et al., 2006), whereas only a few papers on bacterial pathogen–plant interactions were reported (Mehta and Rosato, 2001).

Bacterial blight, a disease caused by *Xoo* affecting rice deleteriously, poses a significant agronomic problem in many rice-growing regions and is an ideal model system for the study of the interaction between plants and their bacterial pathogens (Gu et al., 2005). In this study, we applied 2-DE to investigate changes in protein level involving in incompatible interactions between a stable bacterial blight resistant somatic hybrid line (regenerated from fusion between *Oryza meyeriana* L. and a *japonica* rice cultivar) and bacterial pathogen *Xoo*.

* Corresponding author. Tel.: +86 579 82282949; fax: +86 579 82282269.
E-mail address: yangl@zjnu.cn (L. Yang).

0031-9422/$ - see front matter © 2008 Elsevier Ltd. All rights reserved.
doi:10.1016/j.phytochem.2008.04.006

2. Results and discussion

2.1. SH76 exhibiting a strong resistance to Xoo

The wild rice *O. meyeriana* shows high immunity to bacterial blight. To improve the resistance of cultivated rice to *Xoo*, we introduced a bacterial blight resistance trait from this wild rice species into a japonica rice cultivar (8411) using asymmetric somatic hybridization (Yan et al., 2004). A stable somatic hybrid line SH76 (BC_1F_8, backcrossed with 8411) had a wide-spectrum resistance against ten Philippine (from P1 to P10) and four Chinese (III, IV, V and VI) *Xoo* strains (unpublished data of our laboratory). A strongly virulent *Xoo* strain Chinese pathotypes IV (Zhe173), which is widely distributed across China and Southeast Asia, was used to study incompatible interaction. Both SH76 and 8411 rice seedlings were inoculated with Zhe173 by clipping method. Visible symptoms on 8411 and SH76 leaves were observed at 6 and 12 days after inoculation, respectively. The discoloration on 8411 leaves persisted and become more severe at 17 days, and spread over a major part of the leaf blade (Fig. 1a). In susceptible 8411 leaves, Zhe173 vigorously increased after 2 days inoculation, reaching to 4763333 cfu/mL at 6 days after inoculation. In resistant SH76 leaves, the population of Zhe173 decreased after 3 days inoculation although increased significantly ($p < 0.01$) at 3 days after inoculation (Fig. 1b). Theses results indicated that SH76 exhibited a hypersensitive response against Zhe173 that severely restricted bacterial growth.

2.2. Identification of differentially expressed proteins in rice leaves during early responses to Xoo

To investigate early responses in protein level of SH76 before any disease symptoms, plants were selected for proteomic analysis at 24, 48, and 72 h after *Xoo* inoculation. In order to distinguish resistant responses from developmental changes in protein expression, both mock and *Xoo* inoculated leaves were harvested at each time point of treatment. More than 900 protein spots were reproducibly detected by PDQuest 7.3 software on silver-stained gels. The representative 2-DE maps are shown in Fig. 2, in which two framed regions are enlarged in Fig. 3. The proteins were separated completely in both dimensions. Quantitative image analysis revealed a total of 77 protein spots that changed their intensities significantly ($p < 0.05$) by more than 1.5-fold at least at one time point. The Venn diagram was used to indicate the differentially expressed spots at three time points (Fig. 4). Seventeen spots were differentially expressed at all three time points, 8 at both 24 h and 48 h, 20 at both 48 h and 72 h, 31 only at 48 h and 1 only at 24 h. Among 77 protein spots, 76 were differentially expressed at

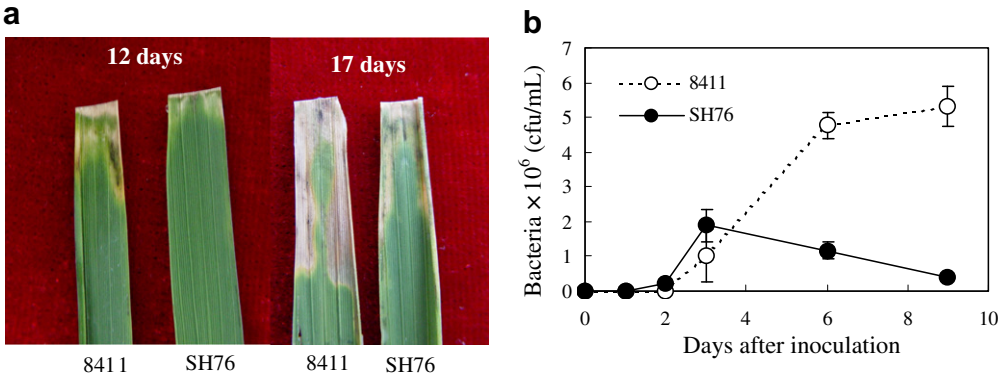

Fig. 1. The effect of *Xoo* inoculation on rice seedlings. Five-leaf stage seedlings were inoculated with Zhe173 of *Xoo* by clipping method. Symptom changes in susceptible 8411 and resistant SH76 leaf segments at 12 and 17 days postinoculation (a). The population of Zhe173 after inoculation was determined by the plate colony counting methods (b). Values are the mean ± SE of bacterial populations from three leaf blades.

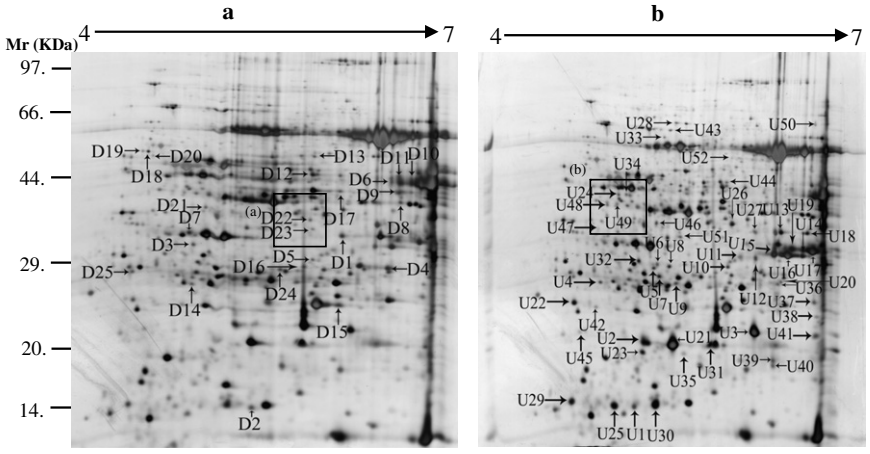

Fig. 2. Representative 2-DE gels of rice leaf proteins at 48 h time points. Twenty-five down-regulated spots are indicated in the map of control sample (a) and 52 up-regulated spots are indicated on the map of *Xoo* -inoculated sample after 48 h (b). The framed regions are enlarged in Fig. 3.

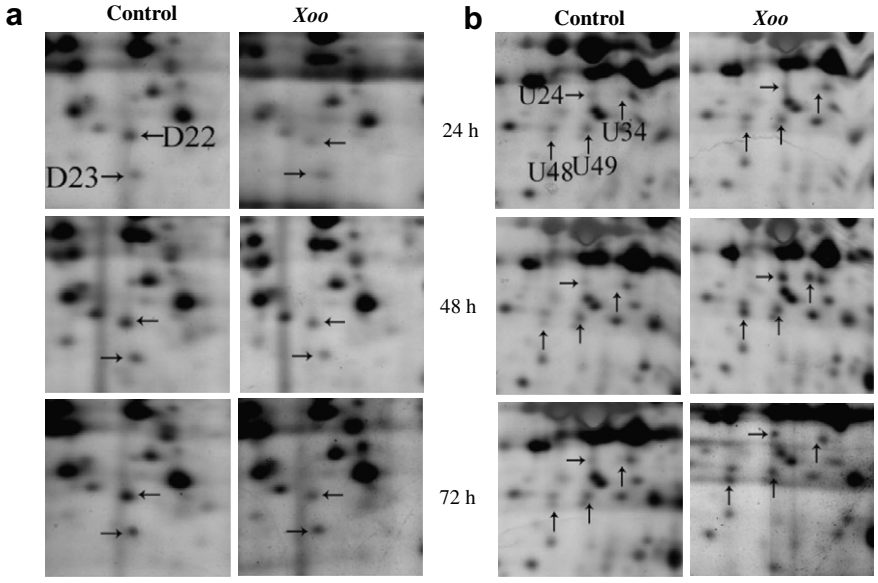

Fig. 3. Time-dependent changes of the differentially expressed protein spots. Proteins in leaves were extracted from control and *Xoo* -inoculated samples after 24, 48 and 72 h treatment and separated by 2-DE. (a) and (b) correspond to the framed regions (a) and (b) in Fig. 2.

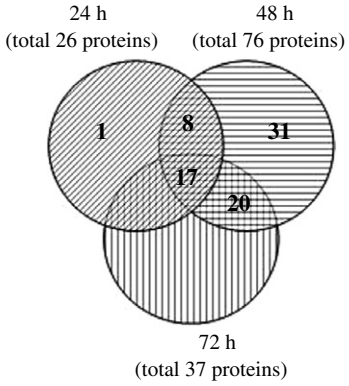

Fig. 4. Classification of the proteins on the basis of their differential expression at three time points. The number of differentially expressed spots at a particular time point is shown in the different segments.

48 h time point. These results suggest that 48 h may be the pivotal time point for the incompatible interaction between rice and *Xoo* in protein level.

The differentially expressed proteins at 48 h after inoculation were excised from the preparative gels, in-gel digested by trypsin, and analyzed by a MALDI-TOF/TOF mass spectrometer. A search was conducted for the acquired PMF data against NCBInr database. The Mascot score cut-off point for a positive identification was 60. In total, 64 protein spots were successfully identified by PMF analysis (Table 1).

2.3. Functional classification and subcellular localization prediction of *Xoo*-responsive proteins

While most of 64 identified proteins were well-known pathogen-responsive proteins (Mahmood et al., 2006), three including phytosulfokine receptor precursor (U36), CHP-rich zinc finger protein (U48), and auxin-regulated protein (U46), were first reported to be involved in the plant–pathogen interaction. Fifty-one proteins of known functions were classified into five functional categories including photosynthesis, antioxidant defense, protein turnover, signal transduction, and metabolisms (Fig. 5).

Pathogen invasion will trigger the signal transduction cascades that eventually lead to activation of pathogen-responsive genes. Five identified proteins were included in signal transduction: phytosulfokine receptor precursor (U36) (Matsubayashi et al., 2006), G protein (U9) (Ono et al., 2001), phosphatidylinositol 3-kinase-related protein kinase (D22) (Katso et al., 2001), CHP-rich zinc finger protein (U48) (Korfhage et al., 1994) and auxin-regulated protein (U46) (Liscum and Reed, 2002) (Table 1). In the other proteomic analysis, Mahmood et al. (2006) did not identify any proteins related to signal transduction at 72 h after *Xoo* inoculation. The results indicated that protein expression changes at 48-h time point were early responses to *Xoo* infection.

In many incompatible interactions, oxidative burst or increase in ROS is often the first detectable response (Mahmood et al., 2006). Upon pathogen attack, ROS can help to induce hypersensitive death of infected cells or serve as a signal to activate defense responses in distant uninfected cells (Hammond-Kosack and Parker, 2003). However, the ROS species also cause damage to cellular components. Plants can control the ROS level through sophisticated mechanisms such as scavenging them by antioxidant defense proteins (Mahmood et al., 2006). Here three identified proteins belong in this category: ascorbate peroxidase (U4), glutathione S-transferase (U7) and mitochondrial chaperonin-60 (U43). All three proteins were up-regulated by *Xoo* infection (Table 1), which may act together to fight against the ROS produced under the pathogen invasion (Cabiscol et al., 2002; Shigeoka et al., 2002).

2.4. Thirty-five photosynthetic protein spots changed by Xoo infection

Several pathogens have been found to suppress photosynthesis of the host. In contrast, some pathogens pursue an alternative strategy maintaining photosynthesis of the host in green islands of the leaves (Berger et al., 2007). As for photosynthetic responses induced by *Xoo* in rice leaves, information on this topic is limited. The largest functional category was proteins involved in photosynthesis (55%) (Fig. 5) and the majority of them are RcbL. As Table 1 shown, a total of 25 protein spots with different *Mr* values were from the RcbL family. These spots must be RcbL fragments because *Mr* value observed were much smaller than the theoretical one.

Table 1
Differentially expressed proteins at 48 h time points identified by PMF

Spot No.	Accession number	Annotation	V[a]	S[b]	M[c]/C[d](%)	L[e]	Theor./Exp.	
							Mr (kDa)	p*I*
Photosynthetic proteins								
U1	P12089	Rubisco large chain precursor	3.0 ± 0.46	100	22/25	~	52.8/15.3	6.22/5.24
U2	P12089	Rubisco large chain precursor	2.9 ± 0.25	72	13/30	~	52.8/15.3	6.22/5.24
U3	AAP53258	Putative RbcL	2.4 ± 0.10	85	14/23	~	52.9/22.5	6.45/6.28
U5	BAA02730	Chloroplastic aldolase	5.8 ± 0.22	114	17/34	C	42.1/30.1	7.60/5.41
U10	Q8S0J7	Probable membrane-associated 30 kDa protein, chloroplast precursor	2.8 ± 0.22	177	20/60	C	35.1/29.8	9.30/6.08
U11	P12089	Rubisco large chain precursor	1.6 ± 0.14	196	31/54	~	52.8/32.7	6.22/6.16
U12	P12089	Rubisco large chain precursor	1.5 ± 0.14	216	37/47	~	52.8/32.5	6.22/6.29
U14	P12089	Rubisco large chain precursor	on	170	28/51	~	52.8/32.9	6.22/6.70
U15	P12089	Rubisco large chain precursor	3.1 ± 0.15	160	34/40	~	52.8/33.2	6.22/6.44
U16	P12089	Rubisco large chain precursor	2.6 ± 0.20	157	33/43	~	52.8/32.8	6.22/6.57
U17	P12089	Rubisco large chain precursor	3.2 ± 0.11	151	35/40	~	52.8/32.9	6.22/7.70
U18	P12089	Rubisco large chain precursor	6.4 ± 0.38	151	24/47	~	52.8/37.0	6.22/6.47
U19	P12089	Rubisco large chain precursor	5.2 ± 0.32	212	36/48	~	52.8/34.0	6.22/6.60
U20	YP_654221	Rubisco large chain	2.5 ± 0.25	122	27/38	~	52.8/28.8	6.22/6.51
U21	P12089	Rubisco large chain precursor	1.8 ± 0.18	65	10/24	~	52.8/21.1	6.22/5.57
U23	P12089	Rubisco large chain precursor	2.2 ± 0.19	70	10/21	~	52.8/20.1	6.22/5.31
U24	XP_478741	Putative peptidyl–prolyl *cis–trans* isomerase protein	on	117	16/41	C	49.8/45.0	5.64/5.11
U25	P12089	Rubisco large chain precursor	4.8 ± 0.09	81	19/27	~	52.8/15.3	6.22/5.07
U26	P93431	RCA, Ribulose bisphosphate carboxylase/oxygenase activase	1.5 ± 0.10	120	23/42	C	47.8/38.7	5.85/6.09
U27	P12089	Rubisco large chain precursor	on	115	20/42	~	52.8/37.1	6.22/6.28
U29	P12089	Rubisco large chain precursor	1.5 ± 0.11	61	12/24	~	52.8/15.7	6.22/4.71
U35	NP_911136	Probable photosystem II oxygen- evolving complex protein 2 precursor	4.7 ± 0.30	79	7/26	C	26.9/20.2	8.66/5.67
U39	YP_654221	Rubisco large chain	on	161	30/36	~	53.6/19.3	6.33/6.44
U40	YP_654221	Rubisco large chain	on	121	26/29	~	53.6/18.7	6.33/6.44
U45	2002393A	Oxygen-evolving complex protein 1	on	129	13/63	C	26.5/22.3	5.13/4.78
D1	NP_920971	Putative RbcL	0.4 ± 0.05	108	20/36	~	52.9/39.4	6.45/6.22
D2	YP_654212	ATPase alpha subunit, 3′-partial	0.3 ± 0.07	120	16/50	M	29.3/15.2	5.27/5.58
D3	AAO22559	Sedoheptulose-1,7-bisphosphatase precursor	0.4 ± 0.11	66	14/28	C	42.2/33.3	5.83/5.17
D4	NP_920971	Putative RbcL	0.2 ± 0.05	154	20/37	~	52.9/29.9	6.45/6.53
D6	P12089	Rubisco large chain precursor	0.3 ± 0.09	102	19/40	~	52.8/46.1	6.22/6.46
D7	2002393A	Oxygen-evolving complex protein 1	0.3 ± 0.08	192	18/68	~	26.5/35.3	5.13/5.14
D8	P12089	Rubisco large chain precursor	0.5 ± 0.09	86	14/30	~	52.8/40.9	6.22/6.61
D9	P12089	Rubisco large chain precursor	0.2 ± 0.04	90	16/34	~	52.8/42.8	6.22/6.61
D10	P12089	Rubisco large chain precursor	0.1 ± 0.02	145	22/45	~	52.8/46.3	6.22/6.61
D11	P12089	Rubisco large chain precursor	0.1 ± 0.04	165	34/40	~	52.8/46.3	6.22/6.55
Protein turnover								
D12	XP_470417	Translational elongation factor Tu	0.4 ± 0.12	175	24/58	M	48.4/47.9	6.04/6.04
D25	ABA94696	Proteasome subunit alpha type 5	0.5 ± 0.08	121	15/59	~	26.0/29.6	4.70/4.72
Metabolism								
U28	NP_915977	Putative 2,3-bisphosphoglycerate- independent phosphoglycerate mutase	2.2 ± 0.11	161	22/47	~	55.9/67.5	5.40/5.56
U34	XP_493811	Glyceraldehyde-3-phosphate dehydrogenase b subunit	on	86	14/38	C	47.1/45.0	6.22/5.17
U44	XP_493811	Glyceraldehyde-3-phosphate dehydrogenase *b* subunit	on	168	24/48	C	47.1/47.1	6.22/5.64
U49	NP_921034	Putative acetyl-CoA carboxylase	3.1 ± 0.66	76	28/33	C	25.2/42.9	5.02/5.10
U52	AAA84588	ATP synthase β chain	on	122	20/36	~	53.9/54.2	5.30/6.09
D17	NP_921996	Cytoplasmic malate dehydrogenase	0.5 ± 0.06	88	14/53	~	35.5/43.3	5.75/6.19
Signal transduction								
U9	XP_470098	Putative GTP-binding protein	1.5 ± 0.07	78	15/27	M	63.6/28.6	10.12/5.42
U36	NP_912235	Phytosulfokine receptor precursor	on	60	13/29	C	50.5/28.4	9.58/6.48
U46	XP_483757	Putative auxin-regulated protein	2.7 ± 0.17	106	17/57	M	37.1/38.9	6.84/5.43
U48	XP_478653	CHP-rich zinc finger protein-like	6.7 ± 0.23	81	10/44	C	28.2/42.7	4.89/5.01
D22	XP_469649	Putative phosphatidylinositol 3-kinase-related protein kinase	0.4 ± 0.06	59	31/9	M	38.4/37.7	6.01/5.98

Antioxidant defense proteins								
U4	XP_479627	Ascorbate peroxidase	3.5 ± 0.49	133	18/63	~	27.1/28.8	5.21/4.95
U7	NP_922478	Putative glutathione S-transferase	2.0 ± 0.08	106	15/44	~	25.7/29.6	5.34/5.46
U43	NP_921872	Mitochondrial chaperonin-60	1.5 ± 0.06	288	37/59	M	60.8/67.5	5.71/5.56
Other/unclassified								
U6	XP_462957	Putative hydrolase	2.6 ± 0.29	83	7/27	C	40.8/31.5	9.17/5.44
U8	NP_920080	Putative retro element	3.3±0.15	65	13/29	M	47.3/31.2	9.43/5.55
U22	AAP53020	Unknown protein	1.5 ± 0.11	128	17/68	~	16.5/26.0	4.70/4.73
U31	XP_462957	Putative hydrolase	on	92	18/32	C	40.8/20.9	9.17/5.90
U32	XP_462957	Putative hydrolase	1.9 ± 0.24	106	19/25	C	40.8/32.1	9.17/5.28
U42	NP_922898	Putative Mutator protein	2.0 ± 0.13	78	24/16	~	16.7/25.3	5.51/4.91
D13	NP_908684	OSJNBa0011P19.5	0.4 ± 0.08	82	13/40	~	42.9/51.1	5.68/6.02
D14	AAM01152	Putative retro element	0.3 ± 0.10	66	15/32	~	65.5/27.6	9.28/5.16
D15	XP_474551	OSJNBa0022F16.25	0.2 ± 0.07	68	22/28	~	83.1/25.0	4.98/6.17
D18	NP_910024	Hypothetical protein	0.4 ± 0.09	67	9/30	~	31.9/52.5	11.50/4.83
D19	XP_473881	OSJNBa0008M17.5	0.2 ± 0.09	73	24/15	~	20.7/52.6	4.72/4.79
D20	XP_472517	OSJNBa0011E07.12	0.4 ± 0.10	71	26/18	~	16.9/51.4	8.95/4.86
D23	XP_477310	Unknown protein	0.7 ± 0.06	71	19/21	M	94.9/36.2	5.90/6.01

[a] Relative fold change of each spot together with standard deviation. "on" means only detection in the infected samples.
[b] Mascot score.
[c] Number of matched peptides.
[d] Percentage of sequence coverage.
[e] Location. C: chloroplast; M: mitochondrion; ~: any other location.

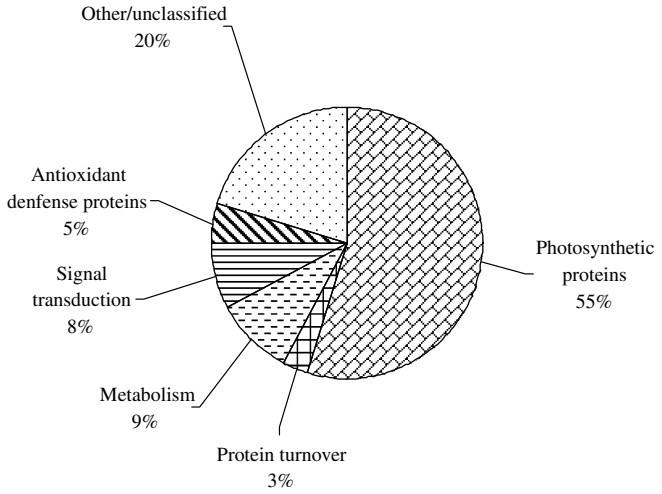

Fig. 5. Functional categories of the identified proteins.

Rubisco keeps a dynamic balance between its intact and degraded forms during normal growth (Zhao et al., 2005). Here, we suggested that accelerated degradation of intact Rubisco and RcbL, and their big fragments occurred upon *Xoo* infection. Therefore, down-regulated spots with about 40 kDa (D1, D8, D9, D10, D11) indicated that the big RcbL fragments were further degraded, and 19 up-regulated fragments with less than 37 kDa were the degration products of intact RcbL and its big fragments (Table 1) (Mahmood et al., 2006). The postulation was further confirmed by Western blot analysis (Fig. 6). The horizontal streak around 55 kDa was Rubisco with multiple p*I* values and intact RcbL, which indeed decreased significantly after *Xoo* inoculation. Six fragments were up-regulated and four were down-regulated by *Xoo* infection. But the amount of fragments detected was not as many as expected. The most probable reason is that the RcbL fragments may lose the antibody recognition site after degradation, so they could not be detected by Western blot analysis.

Using TargetP program, 15 out of 23 protein spots were predicted to be located in the chloroplast (Table 1), implying that the chloroplast is the organelle mostly affected by *Xoo* infection. As we all know, Rubisco in chloroplasts is a major player in photosynthesis. Once ROS accumulate in chloroplasts, Rubisco may be modified, facilitating its subsequent degradation by proteases (Zhao et al., 2005). Although two components of oxygen-evolving complex protein (OEC1, U45; OEC2, U35) were up-regulated by *Xoo* infection, they may be the degraded fragments of D7 or others because their experimental *Mr* were significantly lower than their theoretical values (Table 1). It has recently been reported that the OEC may be the primary site of photoinhibition of PSII, with oxidative damage to the D1 polypeptide once the OEC is unable to supply electrons to reduce oxidized $P680^+$ (Ingle et al., 2007). Thus, the decrease in OEC1 (D7) protein level could represent degradation caused by *Xoo* invasion (Mahmood et al., 2006). Degradation of photosynthetic apparatus, RcbL and OEC, may contribute to accelerate hypersensitive death of *Xoo*-infected cells (Boccara et al., 2007) and confine the pathogen by stopping it from spreading and to trigger local and systemic signaling for the activation of defenses in noninfected cells.

On the other hand, the abundance of three proteins involved in photosynthesis was significantly increased at 48 h infection: peptidyl–prolyl *cis–trans* isomerase (U24), Rubisco activase (RCA, U26), and chloroplastic aldolase (U5) (Table 1). Peptidyl–prolyl *cis–trans* isomerase was a cyclophilin-type peptidyl–prolyl *cis–trans* isomerase, similar to the spinach thylakoid lumen protein TLP40. It had been demonstrated that TLP40 up-regulated the activity of a PSII-

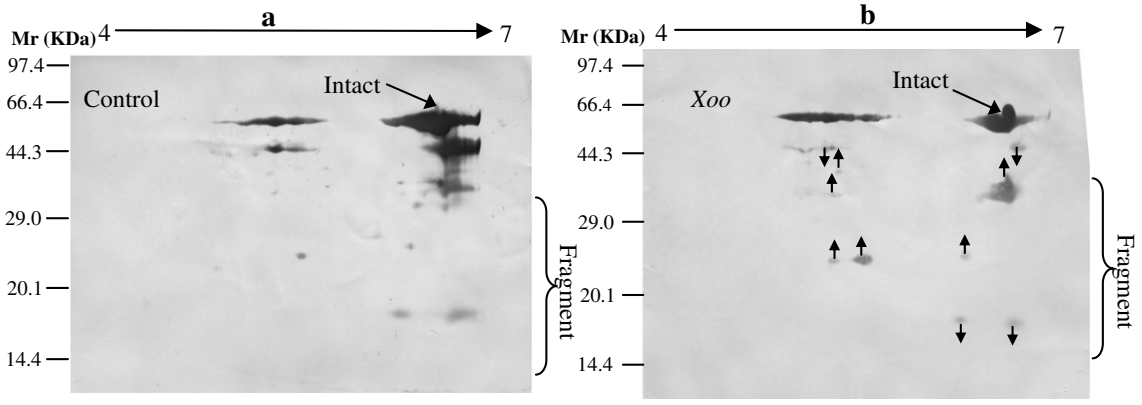

Fig. 6. Western blotting analysis of Rubisco large subunit (RcbL). The total proteins from the control (a) and the sample at 48 h after *Xoo -infection* (b) were separated by 2-DE. Both the intact RcbL and the fragments were detected by anti-RcbL antibody. Up-regulation (↑) and down-regulation (↓) indicated on *Xoo* -infection gel.

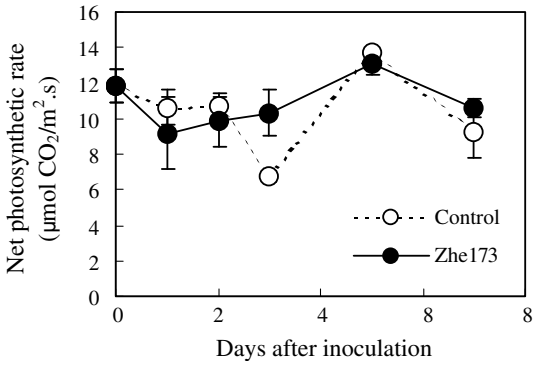

Fig. 7. Net photosynthetic rate of inoculated leaves.

specific protein phosphatase within the thylakoid membrane (Vener et al., 1999). The activation of the membrane protein phosphatase can trigger accelerated repair of photo-damaged PSII (Rokka et al., 2000). RCA, a molecular chaperone, catalyzes Rubisco from an inactive closed conformation to an active open conformation. Transgenic plants with drastically reduced amounts of RCA had lower rates of net photosynthesis (Salvucci et al., 2006). Chloroplastic aldolase catalyses a readily reversible reaction in the Calvin cycle. It was found that even a moderate decrease in the activity of chloroplastic aldolase resulted in the inhibition of photosynthesis, alters the levels of sugars and starch, and inhibits growth of potato plants (Haake et al., 1998). These three pivotal proteins were up-regulated by *Xoo* infection, which would promote the photosynthetic efficiency at non-infection cells. This postulation was confirmed by photosynthetic rate (Fig. 7). Although the photosynthetic apparatus were degraded after *Xoo* inoculation, the net photosynthetic rate of inoculated leaves did not decreased significantly (Fig. 7), which help to activate systemic increases in pathogen resistance.

3. Concluding remarks

Plants exhibit resistance against incompatible pathogens, via localized and systemic responses as part of integrated defense mechanisms. Comparative proteomic analysis of the rice somatic hybrid identified 77 differentially expressed proteins, which may play a role in incompatible interaction with *Xoo.* Our study supports that chloroplasts are key players in plant defense. The loss of integrity of photosynthetic apparatus, specifically RcbL, may be the source of the hypersensitive response and would also lead to limited amounts of available simple sugars, thereby restricting pathogen growth. In other words, bacterial blight resistant somatic hybrid plants response to *Xoo* pathogens not only increase local programmed cell death at infected cells, but also induce systemic pathogen resistance at non-infection cells following *Xoo* infection. How plants regulate the destruction of photosynthetic apparatus and increases of systemic pathogen resistance during defense remains unclear and further studies required.

4. Experimental

4.1. Plant material

Seeds of SH76, a stable bacterial blight resistant somatic hybrid of *Oryza meyeriana* L., a wild rice species, and a *japonica* rice cultivar 8411 (Yan et al., 2004), were surface-sterilized and allowed to germinate in the dark for 48 h. Rice seedlings were grown in a growth chamber with 28/25 °C (day/night), photon flux density of 350–400 μmol m^{-2} s^{-1}, 16 h photoperiod, and relative humidity of 60–80%. Five-leaf stage seedlings were used in the experiment.

4.2. Pathogen inoculation

The incompatible *Xoo* strain Zhe173, a typical one in Yangtze River valley in China, was used in this study. Zhe173 inoculum was prepared from 48 h culture on PSA slants and its density was adjusted to 10^9 CFU/ml. After clipping the tip (about 1 cm) of the fully expanded uppermost leaf with scissor dipped into the inoculum, the seedlings were incubated in the growth chamber at 28 °C. The inoculated leaves were harvested at 24, 48, and 72 h after inoculation. As a control, mock-inoculated plants were treated under the same conditions with the exception of the pathogen inoculum was replaced with sterile water. All leaves were washed to remove surface *Xoo* and 1–2 cm parts near clipping cuts were discarded. Collected tissues from 20 leaves were frozen immediately in liquid nitrogen and stored at −70 °C.

4.3. Net photosynthetic rate

Net photosynthetic rate of the inoculated leaf was measured using a GFS-3000 portable photosynthesis system (WALZ, Effeltrich, Germany). Measurements were carried out with a light intensity of 800 μmol/m^2 s, a CO_2 concentration of 500 ppm, and a temperature 27 ± 1 °C. Three sub-measurements were made on three different plants.

4.4. Protein extraction and 2-DE

The leaf proteins were extracted using trichloroacetic acid/acetone method (Yan et al., 2005). Protein concentration was estimated with Bradford method using BSA as standard. For the first dimension separation, pH 4–7 IPG strips (17 cm, linear, Bio-Rad) were initially rehydrated with protein samples for 12 h. IEF was carried out in the Bio-Rad PROTEAN IEF Cell. Focusing was performed in four steps: 250 V for 30 min, 1000 V for 1 h, 10,000 V for 5 h and 10,000 V for 90 kVh. Every IPG strip was equilibrated in 5 mL equilibration buffer I (6 M urea, 50 mM Tris–HCl buffer, pH 8.8, 2% w/v SDS, 20% v/v glycerol, 2% w/v DTT) and 5 mL equilibration buffer II (6 M urea, 50 mM Tris–HCl buffer, pH 8.8, 2% w/v SDS, 20% v/v glycerol, 2.5% w/v iodoacetamide) for 15 min, respectively. The second dimension separation was performed with 12% polyacrylamide gels using the PROTEAN® Plus Dodeca system (Bio-Rad). These gels were initially run at 15 mA per gel for 30 min and followed by 30 mA per gel until the bromophenol blue reached the bottom of the gels. For 2-DE, 250 μg and 2 mg of proteins were loaded onto analytical and preparative gels, respectively. Protein spots in analytical gels were visualized by silver staining (Yan et al., 2000), and preparative gels were stained with colloidal CBB G-250 (Candiano et al., 2004). At least triplicate gels were performed for each sample.

4.5. Gel scanning and image analysis

The stained gels were scanned at 500 dots per inch resolution using a UMAX Power Look 2100XL scanner (Maxium Tech., Taipei, China). The transparency mode was used to obtain a grayscale image. Image analysis was conducted according to manufacturer's instructions by using PDQuest 7.3 software (Bio-Rad). First we made some necessary adjustments of the 2D images including rotation and cropping. Spots in the images were then detected and a matchset was created; spots across all gel images in the matchset were automatically matched. Manual edit was also necessary to get a high match rate in the matchset. "Total quantity in valid spots" was used for normalization. In this normalization method, the raw quantity of each spot in a member gel was divided by the total quantity of all the spots in that gel that were included in the master. After finishing the detection and matching of spots, the quality and quantity changes of protein expression were analyzed. In the quantitative sets, the upper limit and the lower limit were set to 1.5 and 0.67, respectively. Student's *t*-test was performed to evaluate the significance level (95%) of quantitative changes between control and each replicate at each time point after *Xoo* inoculation. Only spots with significant and reproducible changes were considered to be differentially expressed proteins.

4.6. In-gel digestion and PMF analysis

Differentially expressed protein spots were manually excised. Tryptic digestion and identification with a 4700 MALDI-TOF-TOF proteomic system (Applied Biosystems) were performed as described previously (Yan et al., 2005, 2006). Briefly, gel spots were digested and desalted with trypsin using the ZipPlate (Millipore, USA). Digested peptides were mixed with α cyano-4-hydroxycinnamic acid and spotted onto MALDI target plates. PMF were collected in positive ion MS reflector mode. The MS spectra were analyzed with a 50 ppm mass tolerance by GPS Explorer V.2.0.1 and Mascot V2.5 based on NCBI and SWISSPROT databases (April, 2006 updated). Background peaks from known trypsin auto-digestion fragments and common keratins were automatically excluded prior to database search. The signal-to-noise criterion was set 25 or greater. The search was performed first taking rice as taxonomy. If no positive results were obtained, the searching was performed again taking green plant as taxonomy. The other parameters for searching were enzyme of trypsin, one missed cleavage; peptide tolerance of 0.15 Da; variable modifications of carbamidomethylation (Cys), oxidation (Met), and pyro-Glu (*N*-terminal Glu); peptide charge of 1+; and monoisotopic. Only significant hits, as defined by the MASCOT probability analysis ($p < 0.05$), were accepted.

4.7. Subcellular localization of proteins

TargetP (www.cbs.dtu.dk/services/TargetP) was used to determine subcellular localization prediction (Zhou et al., 2006).

4.8. Western blotting

Eighty microgram proteins were separated by 2-DE (7 cm, pH 4–7 IPG strips were used for IEF), and transferred onto nitrocellulose membranes using a semidry electrophoretic apparatus (TE 70, Amersham Biosciences). The blotted membranes were blocked for 1 h in TBS (50 mM Tris–HCl, pH 7.5 and 150 mM NaCl) containing 5% (w/v) nonfat dry milk and subsequently incubated with anti-RcbL antibody (a kind gift from Dr. Genyun Chen) at 1:500 dilution for 2 h. The membranes were washed (3×10 min) in TBS. A secondary anti-rabbit IgG antibody conjugated with alkaline phosphatase diluted 1:1000 in TBS was used for immunodetection. After the membranes were washed with TBS (4×5 min), the immunoblot signals were detected using the nitroblue tetra-zolium/5-bromo-4-chloro-3-indolyl phosphate method.

Acknowledgements

The authors wish to thank Dr. GenYun Chen (Institute of Plant Physiology and Ecology, Chinese Academy of Sciences) for the gift of the anti-RcbL antibody, and Ho Yin Leung (University of California at San Diego) for critical reading and grammatical correction of manuscript. This work was supported by grants from National Natural Science Foundation of China (Grant 30471074) and Natural Science Foundation of Zhejiang Province (Grant Y304047).

References

Berger, S., Benediktyova, Z., Matous, K., Bonfig, K., Mueller, M.J., Nedbal, L., Roitsch, T., 2007. Visualization of dynamics of plant–pathogen interaction by novel combination of chlorophyll fluorescence imaging and statistical analysis: differential effects of virulent and avirulent strains of *P. syringae* and of *oxylipins* on *A. thaliana*. J. Exp. Bot. 58, 797–806.

Boccara, M., Schwartz, W., Guiot, E., Vidal, G., De Paepe, R., Dubois, A., Boccara, A.C., 2007. Early chloroplastic alterations analysed by optical coherence tomography during a harpin-induced hypersensitive response. Plant J. 50, 338–346.

Cabiscol, E., Bellí, G., Tamarit, J., Echave, P., Herrero, E., Ros, J., 2002. Mitochondrial Hsp60, resistance to oxidative stress, and the labile iron pool are closely connected in *Saccharomyces cerevisiae*. J. Biol. Chem. 277, 44531–44538.

Candiano, G., Bruschi, M., Musante, L., Santucci, L., Ghiggeri, G.M., Carnemolla, B., Orecchia, P., Zardi, L., Righetti, P.G., 2004. Blue silver: a very sensitive colloidal Coomassie G-250 staining for proteome analysis. Electrophoresis 25, 1327–1333.

Chivasa, S., Hamilton, J.M., Pringle, R.S., Ndimba, B.K., Simon, W.J., Lindsey, K., Slabas, A.R., 2006. Proteomic analysis of differentially expressed proteins in fungal elicitor-treated *Arabidopsis* cell cultures. J. Exp. Bot. 57, 1553–1562.

Gu, K.Y., Yang, B., Tian, D.S., Wu, L.F., Wang, D.J., Sreekala, C., Yang, F., Chu, Z.Q., Wang, G.L., White, F.F., Yin, Z.C., 2005. *R* gene expression induced by a type-III effector triggers disease resistance in rice. Nature 435, 1122–1125.

Haake, V., Zrenner, R., Sonnewald, U., Stitt, M., 1998. A moderate decrease of plastid aldolase activity inhibits photosynthesis, alters the levels of sugars and starch, and inhibits growth of potato plants. Plant J. 14, 147–157.

Hammond-Kosack, K.E., Parker, J.E., 2003. Deciphering plant–pathogen communication: fresh perspectives for molecular resistance breeding. Curr. Opin. Biotech. 14, 177–193.

Ingle, R.A., Schmidt, U.G., Farrant, J.M., Thomson, J.A., Mundree, S.G., 2007. Proteomic analysis of leaf proteins during dehydration of the resurrection plant *Xerophyta viscosa*. Plant Cell Environ. 30, 435–446.

Katso, R., Okkenhaug, K., Ahmadi, K., White, S., Timms, J., Waterfield, M.D., 2001. Cellular function of phosphoinositide 3-kinases: implications for development, homeostasis, and cancer. Annu. Rev. Cell Dev. Biol. 17, 615–675.

Kim, S.T., Yu, S., Kim, S.G., Kim, H.J., Kang, S.Y.H., Hwang, D.H., Jang, Y.S., Kang, K.Y., 2004. Proteome analysis of rice blast fungus (*Magnaporthe grisea*) proteome during appressorium formation. Proteomics 4, 3579–3587.

Konishi, H., Ishiguro, K., Komatsu, S., 2001. A proteomics approach towards understanding blast fungus infection of rice grown under different levels of nitrogen fertilization. Proteomics 1, 1162–1171.

Korfhage, U., Trezzini, G.F., Meier, I., Hahlbrock, K., Somssich, I.E., 1994. Plant homeodomain protein involved in transcriptional regulation of a pathogen defense-related gene. Plant Cell 6, 695–708.

Li, Q., Chen, F., Sun, L.X., Zhang, Z.Q., Yang, Y.N., He, Z.H., 2006. Expression profiling of rice genes in early defense responses to blast and bacterial blight pathogens using cDNA microarray. Physiol. Mol. Plant. P. 68, 51–60.

Liscum, E., Reed, J.W., 2002. Genetics of Aux/IAA and ARF action in plant growth and development. Plant Mol. Biol. 49, 387–400.

Mahmood, T., Jan, A., Kakishima, M., Komatsu, S., 2006. Proteomic analysis of bacterial-blight defense-responsive proteins in rice leaf blades. Proteomics 6 (22), 6053–6065.

Matsubayashi, Y., Ogawa, M., Kihara, H., Niwa, M., Sakagami, Y., 2006. Disruption and overexpression of Arabidopsis phytosulfokine receptor gene affects cellular longevity and potential for growth. Plant Physiol. 142, 45–53.

Mehta, A., Rosato, Y.B., 2001. Differentially expressed proteins in the interaction of *Xanthomonas axonopodis* pv. *citri* with leaf extract of the host plant. Proteomics 1, 1111–1118.

Ono, E., Wong, H.L., Kawasaki, T., Hasegawa, M., Kodama, O., Shimamoto, K., 2001. Essential role of the small GTPase Rac in disease resistance of rice. Proc. Natl. Acad. Sci. USA 98, 759–764.

Rokka, A., Aro, E.M., Herrmann, R.G., Andersson, B., Vener, A.V., 2000. Dephosphorylation of photosystem II reaction center proteins in plant photosynthetic membranes as an immediate response to abrupt elevation of temperature. Plant Physiol. 123, 1525–1535.

Salvucci, M.E., DeRidder, B.P., Portis Jr., A.R., 2006. Effect of activase level and isoform on the thermotolerance of photosynthesis in *Arabidopsis*. J. Exp. Bot. 57, 3793–3799.

Shigeoka, S., Ishikawa, T., Tamoi, M., Miyagawa, Y., Takeda, T., Yabuta, Y., Yoshimura, K., 2002. Regulation and function of ascorbate peroxidase isoenzymes. J. Exp. Bot. 53, 1305–1319.

Smith, K.P., Handelsman, J., Goodman, R.M., 1999. Genetic basis in plants for interactions with disease suppressive bacteria. Proc. Natl. Acad. Sci. USA 96, 4786–4790.

Vener, A.V., Rokka, A., Fulgosi, H., Andersson, B., Herrmann, R.G., 1999. A cyclophilin-regulated PP2A-like protein phosphatase in thylakoid membranes of plant chloroplasts. Biochemistry 38, 14955–14965.

Yan, C.Q., Qian, K.X., Xue, G.P., Wu, Z.C., Chen, Y.L., Yan, Q.S., Zhang, X.Q., Wu, P., 2004. Production of bacterial blight resistant lines from somatic hybridization between *Oryza sativa* L. and *Oryza meyeriana* L. J. Zhejiang Univ. Sci. 5, 1199–1205.

Yan, J.X., Wait, R., Berkelman, T., Harry, R.A., Westbrook, J.A., Wheeler, C.H., Dunn, M.J., 2000. A modified silver staining protocol for visualization of proteins compatible with matrix-assisted laser desorption/ionization and electrospray ionization-mass spectrometry. Electrophoresis 21, 3666–3672.

Yan, S.P., Tang, Z.C., Su, W.A., Sun, W.N., 2005. Proteomic analysis of salt stress-responsive proteins in rice root. Proteomics 5, 235–244.

Yan, S.P., Zhang, Q.Y., Tang, Z.C., Su, W.A., Sun, W.N., 2006. Comparative proteomic analysis provides new insights into chilling stress responses in rice. Mol. Cell. Proteomics 5, 484–496.

Zhao, C.F., Wang, J.Q., Cao, M.L., Zhao, K., Shao, J., Lei, T., Yin, J., Hill, G.G., Xu, N., Liu, S., 2005. Proteomic changes in rice leaves during development of field-grown rice plants. Proteomics 5, 961–972.

Zhou, W., Eudes, F., Laroche, A., 2006. Identification of differentially regulated proteins in response to a compatible interaction between the pathogen *Fusarium graminearum* and its host, *Triticum aestivum*. Proteomics 6, 4599–4609.